The Nanoelectronic Modeling Tool NEMO 5: Capabilities, Validation, and Application to Sb-Heterostructures

Sebastian Steiger[1], Michael Povolotskyi[1], Hong-Hyun Park[1], Tillmann Kubis[1], Ganesh Hegde[1], Benjamin Haley[1], Mark Rodwell[2] and Gerhard Klimeck[1,3]

[1]Network for Computational Nanotechnology, Purdue University, West Lafayette IN 47906, USA

[2]University of California, Santa Barbara, CA 93106, USA

[3]Email: gekco@purdue.edu. Phone: (765) 494-9212

Introduction

Modeling and simulation take an important role in the exploration and design optimization of novel devices. As the downscaling of electronic devices continues, the description of interfaces, randomness, and disorder on an atomistic level gains importance and continuum descriptions lose their validity. Often a full-band description of the electronic structure is needed to model the interaction of different valleys and nonparabolicity effects. NEMO 5 [1] is a modeling tool that addresses these issues and is able to provide insight into a broad range of devices. It unifies the capabilities of prior projects: multiscale approaches to quantum transport in planar structures in NEMO-1D [2], multimillion-atom simulations of strain and electronic structure in NEMO-3D [3] and NEMO-3D-Peta [4], and quantum transport in nonplanar structures in OMEN [5]. NEMO 5 aims at becoming a community code whose structure, implementation, resource requirements and license allow experimental and theoretical researchers in academia and industry alike to use and extend the tool.

Capabilities and Validation

NEMO 5 currently handles pseudomorphic nanostructures composed of diamond, zincblende, simple-cubic, wurtzite, graphene and rhombohedral (trigonal) crystals. It is able to compute *strain* in large structures using an enhanced valence force field model [6] (Fig. 1). The same physical model can be used to find *phonon* spectra (Fig. 2). These capabilities have been validated against various literature results [7].

Electronic structure calculations are done using the empirical tight-binding method [8] using a variety of nearest-neighbor models ranging from an effective mass description to the 20-band $sp^3d^5s^*$ model. Bulk band structures for most IV and III-V materials were validated against literature results. Band diagrams of nanostructures were shown to coincide with independently developed codes. The influence of strain can be treated using the formulation of Ref. 9 or an enhanced version [10]. *Quantum Dot Lab* [11], an educational version of an effective mass solver with interactive 3D wavefunction and absorption visualization that uses NEMO 5 as an engine, is available online at *nanoHUB.org* without the need for any installation.

Selfconsistent *Schroedinger-Poisson* calculations can be performed using a multiscale approach where the density can be based on a mixture of quantum and semiclassical models. This enables the simulation of larger structures where the computationally intensive solution of the Schrödinger equation is restricted to the central parts. A 1D version of this capability can be accessed online [12] through *nanoHUB.org* (Fig. 3). This type of simulation was also validated with independently developed code.

Quantum transport through nanostructures can be computed using two approaches. For ballistic, coherent calculations an open-boundary wavefunction method is preferred [13] (Fig. 4). These calculations have been validated against literature [14] and prior developed code [5]. Electron-phonon scattering can be included in a deformation-potential description [15] using the NEGF formalism [14].

Application: Sb heterostructures

As an example application we present band structure calculations of two antimonide-based heterostructures. [111]-Sb heterostructures were recently proposed as high-current HEMT candidates [16]. The relative proximity of the Γ-, X- and L-valleys, their coupling through translational symmetry breaking as well as the large anisotropy of carrier masses make the validity of a standard effective mass approach questionable. The calculations in this section were performed using an $sp^3d^5s^*$ tight-binding model including spin-orbit coupling. The parameter sets were determined using genetic-algorithm fitting against literature values for conduction and valence band edges and masses. The fitting process of the parameters including strain effects is still ongoing and the final parameter sets will be published elsewhere [17]. The lattice mismatch of 0.6% (GaSb/AlSb) and 1.3% (InAs/AlSb) is neglected for this work.

In Fig. 5 a triple-QW GaSb-AlSb structure grown along [111] is displayed where the barriers between the wells consist of a single Al-atom. With a lattice constant of 0.61nm, a single [111]-AlSb monolayer has a thickness of about 0.35nm. Although the Γ-valley in bulk GaSb is slightly (30meV) lower than the L-valley, the enormous difference of the effective masses in the confinement direction (0.04 vs. 1.3) pushes the confined Γ-state far above the confined L-state. The high confinement masses also allow for ultrathin barrier layers, enabling exquisite electrostatic control and multiple conduction channels. Yet the in-plane effective masses of the 6 lowest bands remain small such that a fast device can be expected. A series of simulations with well and barrier thicknesses varying between 1 and 3 ML (Table 1) reveals that the in-plane effective masses remain at around 0.09-0.10, close to the bulk value. The masses were obtained by fitting the lowest QW subband within $0.15\pi/a$ of the minimum, as transport in high-current devices occurs above the band edge. A carrier density of $1e13cm^{-2}$ at a temperature of 300K positions the Fermilevel E_F about 70-90meV above the subband edge E_{0L} assuming six parabolic bands. Conversely, $E_F–E_c$~0.2eV is able to accommodate n_{2D}~2-3e13cm^{-2}. As Table 1 illustrates, the separation of higher bands with larger in-plane masses exceeds 0.2eV for most settings.

A second simulation example is the [100]-AlSb/InAs/GaSb/InAs/AlSb single quantum well depicted in Fig. 6a. This heterostructure features no-common-atom interfaces which are preferably of the type In-Sb [18]. The question of tight-binding parameter mixing for the interface bonds has not yet been fully answered. In this work InAs parameters were taken for the In-Sb interface. Especially the split-off valence subband depends on this choice as there are large differences in spin-orbit coupling. The resulting band structure (Fig. 6b) shows large band warping in the valence bands. As expected, the *k=0* eigenfunctions (Fig. 6c) of the conduction band are mostly located in the InAs layers whereas the valence band states are confined to the GaSb layer.

This paper introduces our latest NEMO 5 tool kit to the advanced research community and highlights capabilities relevant to very recent DRC-discussed results [16].

[1] S. Steiger et al., manuscript in preparation.
[2] R. Lake et al., J. Appl. Phys. 81, 7845 (1997)
[3] G. Klimeck et al., IEEE Trans. El. Dev. 54, 2090 (2007)
[4] S. Lee et al., Proc. IWCE 13, 1 (2009)
[5] G. Klimeck and M. Luisier, Proc. IEDM, 1 (2008)
[6] Z. Sui et al., Phys. Rev. B 48, 17938 (1993)
[7] A. Paul et al., J. Comp. Electron. 9, 160 (2010)
[8] G. Klimeck et al., CMES 3, 601 (2002)
[9] T. Boykin et al., Phys. Rev. B 66, 125207 (2002)
[10] T. Boykin et al., Phys. Rev. B 81, 125202 (2010)
[11] DOI: 10254/nanohub-r450.10
[12] DOI: 10254/nanohub-r5203.15
[13] M. Luisier et al., Phys. Rev. B 74, 205323 (2006)
[14] S. Datta, Superlatt. Microstruct. 28, 253 (2000)
[15] S. Jin et al., J. Appl. Phys. 99, 123719 (2006)
[16] M. Rodwell et al., Proc. DRC, 149 (2010)
[17] G. Hegde et al., manuscript in preparation
[18] H. Kroemer, Phys. E 20, 196 (2004)
[19] B. Dorner et al., J. Phys.:Cond. Mat. 2, 1475 (1990)

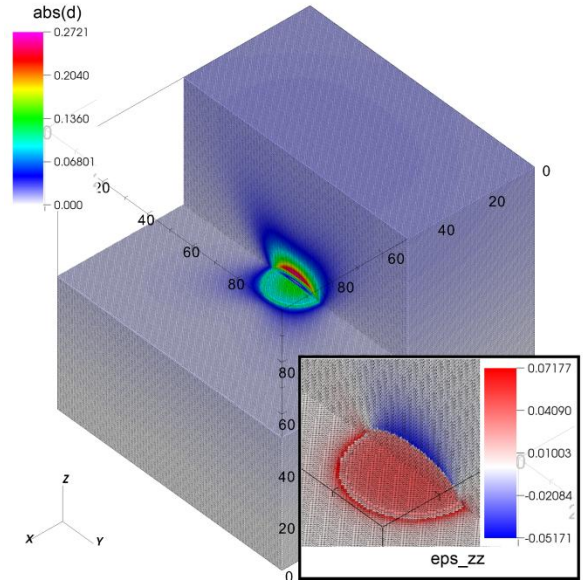

Fig. 1: Strain relaxation in a dome-shaped InAs quantum dot embedded in $(100nm)^3$ GaAs consisting of 44 million atoms. The dot is 20 nm wide and 5 nm high, consisting of about 38000 atoms. Shown is the magnitude of the displacement vector. *Inset:* Strain component ε_{zz}.

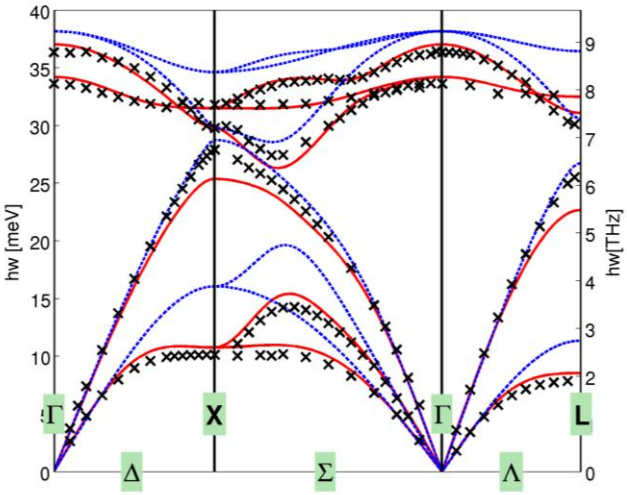

Fig. 2: Bulk phonon dispersions of GaAs computed using the Keating model *(blue – dashed)* and an extended VFF model with augmented Coulomb interaction *(red - solid)*. Also shown are experimental measurements [19] *(black crosses)*.

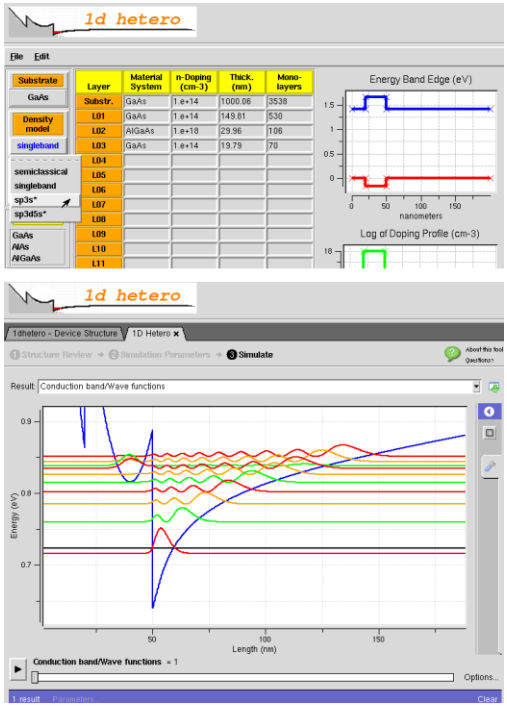

Fig. 3: *1D Heterostructure Design tool* on nanoHUB.org. *Top:* Structure definition screen. *Bottom:* Computed electron states and energies.

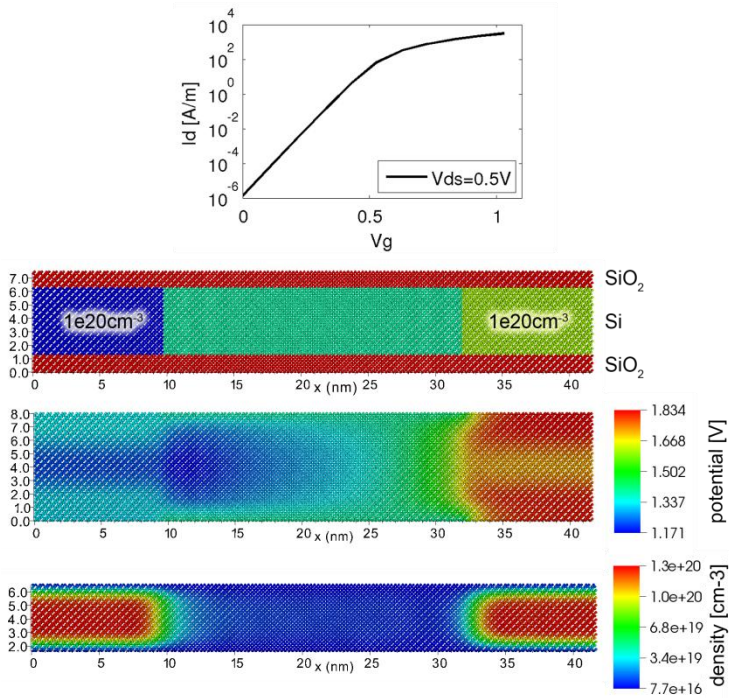

Fig. 4: Transport through an ultrathin-body transistor at Vds=0.5V. *From top to bottom:* Id-Vg curve, schematic of the structure, electrostatic potential and electron density at Vg=0.9V.

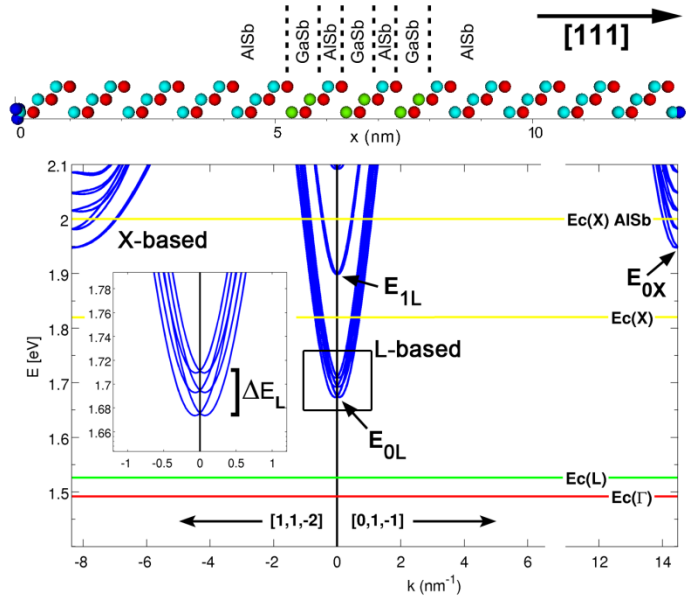

Fig. 5: [111]-GaSb/AlSb triple-QW structure (2 ML wells, 1ML barriers) and in-plane band diagram

AlSb / GaSb	1 ML (0.35nm)	2 ML (0.7nm)	3ML (1.05nm)
1 ML	m*=0.086 ΔE_L=248 ΔE=223	m*=0.088 ΔE_L=50 ΔE=177	m*=0.094 ΔE_L=48 ΔE=152
2 ML	m*=0.105 ΔE_L=35 ΔE=224	m*=0.102 ΔE_L=13 ΔE=270	m*=0.102 ΔE_L=37 ΔE=277
3 ML	m*=0.095 ΔE_L=58 ΔE=240	m*=0.098 ΔE_L=12 ΔE=263	m*=0.100 ΔE_L=9 ΔE=277

Table 1: [111]-GaSb/AlSb triple-QW dependence of m*, the splitting ΔE_L and the distance $\Delta E=\min(E_{0X}, E_{1L})-E_{0L}$ (meV) on well and barrier thicknesses

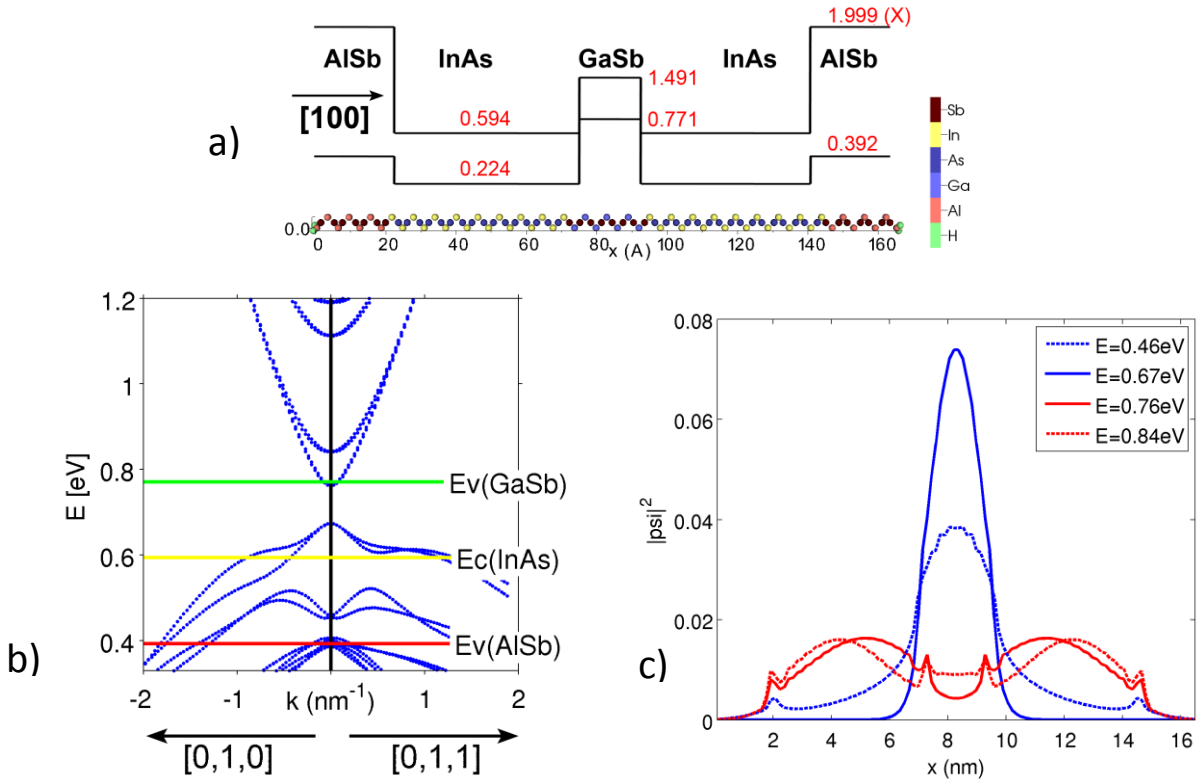

Fig. 6: AlSb/InAs/GaSb/InAs/AlSb double-QW. a) Atomistic structure. b) In-plane band dispersion. c) *k=0* eigenstate wavefunctions for selected energies (average between anion and cation positions).